Journal of Materials Chemistry A

Accepted Manuscript

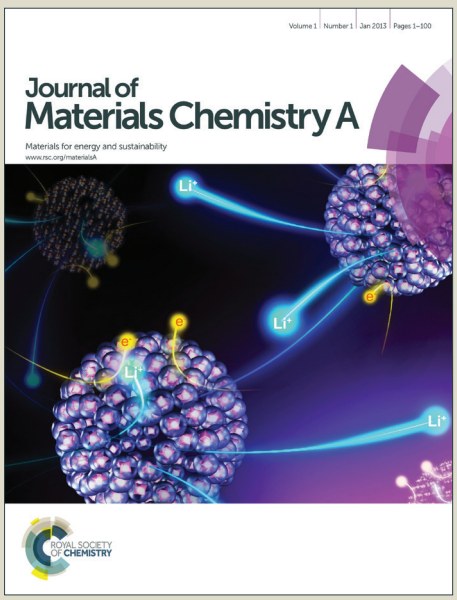

ROYAL SOCIETY OF CHEMISTRY

www.rsc.org/materialsA

Journal of Materials Chemistry A

RSC Publishing

ARTICLE

Low Pressure Induced Porous Nanorods of Ceria with High Reducibility and Large Oxygen Storage Capacity: Synthesis and Catalytic Applications

Cite this: DOI: 10.1039/x0xx00000x

Received 00th January 2012,
Accepted 00th January 2012

DOI: 10.1039/x0xx00000x

www.rsc.org/

Jing Li,[a] Zhiyun Zhang,[a] Zhimin Tian,[a] Xuemei Zhou,[a] Zhiping Zheng,[a, b, c] Yuanyuan Ma,[a, b] Yongquan Qu*[a, b]

Ceria (CeO_2) is finding prolific industrial applications due to its unique redox properties. Such properties, dominated by structural defects that are primarily oxygen vacancies associated with the Ce^{3+}/Ce^{4+} redox couple, can be modulated and optimized by controlling the size and morphology of the material, in particular those that are nanostructured (nanoceria). We report herein a new form of nanoceria prepared by a two-step hydrothermal synthesis. In the first-step hydrothermal treatment, the low reaction pressure is critical for the formation of a $Ce(OH)_3/CeO_2$ precursor. A subsequent hydrothermal step of dehydration and oxidation of the precursor nanorods led to the production of porous nanorods of ceria. The porous nanorods of ceria have been found to display enhanced reducibility and capacity for oxygen storage (900.2 μmol O_2/g) as a result of their significantly increased surface area and defects over other forms of nanoceria, including nanoparticles, non-porous nanorods, nanocubes, and nanooctahedra. Their much improved activities have also been demonstrated in a benchmark reaction – catalytic oxidation of CO. The high catalytic activity of porous nanorods of ceria indicates their potentials as the catalysts or supports or promoters for advanced oxidative processes for waste treatment and environmental remediation.

Introduction

Cerium oxide or ceria (CeO_2) is finding widespread applications due to its unique redox properties, among which its use in automobile catalytic converters is most significant.[1-6] Nanostructured ceria or nanoceria is characterized with a large number of surface-bound defects that are primarily oxygen vacancies and active sites for catalysis.[7-25] All these applications hinge upon how effectively the ceria surface may be reduced and oxygen be stored, that is, how effectively the material can repeatedly pass through Ce^{3+}/Ce^{4+} redox cycles rapidly. This ability of nanoceria to switch between different oxidation states is largely determined by the ratio of surface Ce^{3+}/Ce^{4+} and the concentration of oxygen vacancies.[16, 18-22, 26-28] Much effort has thus been devoted to controlling the concentrations of surface Ce^{3+} and oxygen vacancies, both by chemical doping or post-treatment of ceria and by the production of nanoceria.[12, 29-40] We report herein the preparation and properties of porous nanorods of ceria (*PN*-Ceria), a previously unknown nanostructured form. We found that this novel form of nanoceria possess enhanced reducibility and capacity for oxygen storage, much improved over those reported for other forms of nanoceria and comparable to those of the best-performing ceria-based materials by chemical doping and post-treatments.

Experimental

Preparation of Non-porous Nanorods Precursor

$Ce(NO_3)_3 \cdot 6H_2O$ (1.736 g) and NaOH (19.2 g) were dissolved in 10 and 70 mL of millipore water (MQ water, 18.2 MΩ cm), respectively. The two solutions were thoroughly mixed in a Pyrex bottle and the mixture was aged with continuous stirring for 30 min. Subsequently, the Pyrex bottle was transferred into a temperature-controlled electric oven at 100 °C for 24 hrs. After natural cooling to room temperature, the solid products were collected by centrifugation, and washed with MQ water and ethanol three times, and dried at 60 °C overnight.

Synthesis of Porous Nanorods of CeO_2 (*PN*-CeO_2-160)

The non-porous nanorod precursor (20 mg) was dispersed in 10 mL of MQ water by sonication. The porous nanorods of ceria were obtained under hydrothermal conditions in an autoclave at 160 °C for 12 hrs. The pale-yellow solid products were collected by centrifugation, washed with MQ water and ethanol, and drying at 60 °C overnight.

Synthesis of Porous Nanorods of *PN*-CeO_2-R-160

$Ce(NO_3)_3 \cdot 6H_2O$ (1.736 g) and NaOH (19.2 g) were dissolved in 10 and 70 mL of millipore water (MQ water, 18.2 MΩ cm), respectively. The two solutions were thoroughly mixed in a flask and the mixture was aged under continuous stirring for 30 min. The resulting mixture was then brought up to and maintained under reflux for 24 hrs. After natural cooling to room temperature, the solid products were collected by centrifugation, washed with MQ water and ethanol for three times, and then dried at 60 °C overnight. This non-porous nanorod precursor (20 mg) was dispersed in 10 mL of MQ water by sonication, and the mixture was treated hydrothermally at 160 °C for 12 hrs. The pale-yellow products were collected by centrifugation, washed with MQ water and ethanol, and dried at 60 °C overnight. This obtained sample was labeled as *PN*-CeO_2-R-160, and the "R" means reflux.

Synthesis of Non-porous CeO_2 Nanorods

$Ce(NO_3)_3 \cdot 6H_2O$ (1.736 g) and NaOH (19.2 g) were dissolved in 10 and 70 mL of MQ water, respectively. After aging for 30 min, the mixture was transferred into a stainless steel autoclave for hydrothermal treatment at 100 °C for 24 hrs. The solid products were collected by centrifugation, washed with copious MQ water, and dried at 60 °C overnight.

Synthesis of CeO_2 Nanocubes

The synthesis of CeO_2 nanocubes was similar to that of the non-porous CeO_2 nanorods, but at a higher temperature of 180 °C.

Synthesis of CeO_2 Nanooctahedra

$Ce(NO_3)_3 \cdot 6H_2O$ (434.3 mg) and Na_3PO_4 (1.6 mg) were dissolved in 40 mL of MQ water. This mixture was sonicated for 30 min and then transferred into a stainless steel autoclave which was subsequently sealed and placed in a temperature-controlled electric oven at 170 °C for 12 hrs. After natural cooling to room temperature, the solid products were collected by centrifugation, thoroughly washed by MQ water and ethanol, dried at 60 °C overnight, and then calcinated at 400 °C for 4 hrs.

Synthesis of CeO_2 Nanoparticles

The nanoparticles of ceria were obtained by direct calcination of $Ce(NO_3)_3 \cdot 6H_2O$ in air at 500 °C for 2 hrs.

CO Oxidation

The catalytic activity of the nanoceria was assessed using a home-made fixed bed catalytic reactor. Experimentally, a gas mixture consisting of 1% O_2, 1% CO and 98% Ar was delivered at a flow rate of 50 standard cubic centimeters per minute (sccm) into a quartz tube (i.d. = 4 mm) loaded with 250 mg of the nanoceria catalyst (60-100 mesh) and end-blocked by glass wool. The temperature of catalytic bed was controlled by a K-type thermocouple. The effluent CO and CO_2 were measured using an in-line gas chromatograph equipped with a flame ionization detector (FID). A time interval of 40 min between two data points was allowed to stabilize the reaction temperature.

General Characterization Methods and Equipments

The transmission electron microscopy (TEM) images were obtained with a Hitachi FT7700 instrument at an accelerating voltage of 120 kV. The high-resolution transmission electron microscopy (HRTEM) image and dark-field TEM images were obtained using a JEOL 2100 F instrument with a 200 kV accelerating voltage. Powder X-ray diffraction (XRD) data were collected using a PW 1710 Philips Powder X-ray diffractometer. X-ray photoelectron spectra (XPS) were acquired using a Thermo Electron Model K-Alpha with Al Kα as the excitation source. The surface area was measured by nitrogen physisorption (Quantachrome, Autosorb-iQ) based on the Brunauer-Emmet-Teller (BET) method. Thermogravimetric analysis (TGA) of as-synthesized samples were carried out with Mettler Toledo, STARe at a heating rate of 5 °C/min from room temperature to 800 °C in air. Raman spectra were obtained using a LabRAMHR800 (Horbia Jobin Yvon) instrument at 514 nm. Oxygen storage capacity (OSC) measurement was carried out using CHEMBET-3000 (Quantachrome Co.). The sample (100 mg) for OSC measurement was reduced at 550 °C for 1 h in H_2 (10 mL/min), cooled to 400 °C, and then purged with He (30 mL/min) for 20 min. A given amount of O_2 (0.15 ml) was pulsed every 5 min until the intensity of the peak reached a constant value.

CO Temperature-Programmed Reduction (CO-TPR) Measurements

CO-TPR was carried out in a quartz fixed-bed micro-reactor. For a typical measurement, 50 mg of catalyst was loaded into the reactor. Prior to reactions, the samples were pretreated in argon at 300 °C for 0.5 h. Then, a gas mixture of 5 vol. % CO/Ar (40 mL/min-1) was introduced under a temperature-programmed procedure with a ramping rate of 10 °C /min. The consumption of CO and the accompanying production of CO_2 were monitored by mass spectrometer (QIC-20, HIDEN).

Results and Discussion

PN-Ceria was obtained by a two-step synthesis under hydrothermal conditions as shown in Figure 1. In the first step a mixture of $Ce(NO_3)_3$ and NaOH was hydrothermally treated at 100 °C for 24 hours, affording a non-porous nanorod precursor. Powder X-ray diffraction (XRD, Figure 2j) studies indicated that this precursor is composed of 41.5% of $Ce(OH)_3$ (JCPDS No. 74-0665) and 58.5% of cubic fluorite CeO_2 (JCPDS No. 75-0076). Transmission electron microscopic (TEM) studies revealed its rod-like structure with a dimension of about 8 x 60 nm (Figure 2a). Guided by thermogravimetric analysis with weight loss of 4.1% (TGA, Figure S1), the thoroughly washed precursor was subsequently hydrothermally treated at elevated temperatures. As indicated by XRD analysis, the precursor underwent decomposition/dehydration with its $Ce(OH)_3$ content being transformed into Ce_2O_3, and

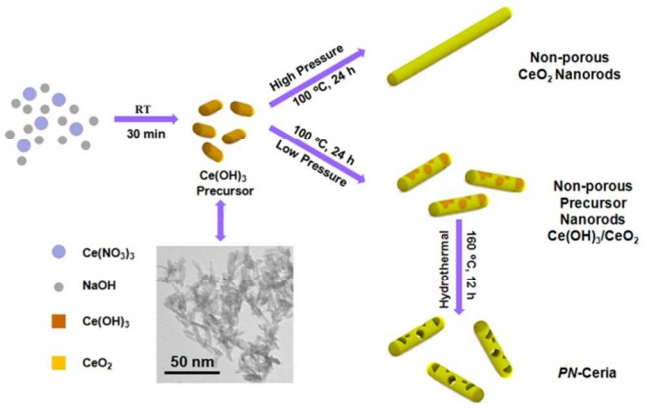

Fig. 1 Schematic of the synthesis of the porous and non-porous CeO_2 nanorods. Experimental results indicate that the low pressure of reaction vessels (~ 1.1 atm) during the hydrothermal at 100 °C is critical to form the non-porous nanorod precursor with the mixed phase of CeO_2 and $Ce(OH)_3$. High pressure of the reaction vessels results in the non-porous CeO_2 nanorods with a large length/diameter ratio. The porous CeO_2 nanorods are prepared by the dehydration of $Ce(OH)_3$ induced by the second hydrothermal at 160 °C in an autoclave.

subsequently to CeO_2, but the precursor-to-CeO_2 conversion was not complete until the temperature reached 160 °C, above which only cubic fluorite CeO_2 was present. Corresponding sequential morphological changes from the precursor to various temperature-dependent phases, denoted as *PN*-Ceria-T with T being the temperature at which the precursor was hydrothermally treated, were revealed by TEM images (Figure 2b-d). The porous feature of nanorods of *PN*-Ceria-160 was clearly revealed by its dark-field TEM image (Figure 2e-f). The absorption/desorption isothermal curves for *PN*-Ceria-160, shown in Figure S2, indicate a Type IV behavior of the nanoporous ceria with a pore volume of 0.45 cm^3/g.[41]

After mixing $Ce(NO_3)_3$ and NaOH at room temperature for 30 min, short rod-like $Ce(OH)_3$ was formed, which was confirmed by TEM images in Figure 1 and XRD results in Figure S3. The pressure under which the reaction mixture was hydrothermally treated appears to be critical. Specifically, when the first step of the reaction was carried out in an autoclave, only non-porous nanorods of ceria were obtained as previously reported (Figure 2g).[29] And an external pressure gauge indicated a pressure inside the autoclave was about 2.0 atm. In the first step of our synthesis, the pressure inside the screw-capped glass vial was about 1.1 atm; this much reduced pressure was probably key to the "arrested synthesis" of the precursor characterized by the presence of $Ce(OH)_3$ that subsequently dehydrated at a higher temperature to produce the present porous nanorods of ceria. The creation and confinement of the pores within the rod-like nanostructure may be understood in terms of the robustness of the precursor nanorods; dehydration, oxidation by the dissolved oxygen, and any accompanying structure reorganization in the hydrothermal treatment were not destructive enough to alter the structural integrity, and hence the preservation of the rod-like morphology.

To further investigate the mechanism possibly responsible for pore formation and to demonstrate the ability to control the resulting porosity, a comparative synthesis was also carried out, first under reflux and ambient atmospheric pressure (1.0 atm) followed by hydrothermal treatment at 160 °C as in the synthesis of *PN*-Ceria-160. A pale-yellow precursor consisting of 25.9% of $Ce(OH)_3$ and 74.1% of CeO_2 was obtained (Figure S4a), and a weight loss of 3.0% between 100 °C to 160 °C in TGA experiment was obtained (Figure S4b). Similar to the synthesis *PN*-Ceria-160, the precursor obtained at 1.0 atm also displayed rod-like morphology (Figure S4c), and subsequent dehydration and oxidation under hydrothermal conditions at 160 °C resulted in porous nanorods (denoted as *PN*-Ceria-R-160, Figure S4d) with a Type IV absorption and desorption isothermal curves (Figure S2) and a smaller pore volume of 0.37 cm^3/g. The lower percentage of $Ce(OH)_3$ can be rationalized in terms of the sufficient amount of O_2 under non-hydrothermal conditions; more Ce^{3+} was oxidized to CeO_2, leaving less Ce^{3+} of the starting $Ce(NO_3)_3$ for the formation of $Ce(OH)_3$. The surface area of *PN*-Ceria-R-160 as determined by Brunauer-Emmett-Teller (BET) analysis is 134 m^2/g. In comparison, the corresponding value of *PN*-Ceria-160 obtained by the two-step synthesis, first at 1.1 atm (for the formation of precursor) and then at 2.0 atm (hydrothermal dehydration and oxidation of the precursor) and directly under 2.0 atm (hydrothermal) is 141 m^2/g. Lending further support to the profound pressure effect on the formation of $Ce(OH)_3$ and the critical significance of its dehydration and oxidation in the formation of the porous nanorods is the smaller surface area of 107 m^2/g for the nanoceria obtained hydrothermally under 2.0 atm without going through the stepwise procedure where reaction pressures differ at the two different stages. The relationship between the surface area of nanocerias and the weight percentage of $Ce(OH)_3$ (as a direct consequence of reaction pressure) is shown in Figure S5, leading to a clear correlation between the reaction pressure and the surface area of the resulting porous nanoceria. Hence, the present results indicate that by controlling the amount of $Ce(OH)_3$ in the precursor, the porosity and the surface area of the nanoporous ceria can be controlled with the key parameter being the reaction pressure.

Using *PN*-Ceria-160 and *PN*-Ceria-R-160 as representatives, the properties of the nanoporous ceria pertinent to the material's applications were investigated by a number of techniques. Aiming at demonstrating their enhanced features and performance, comparative studies using nanoparticles, non-porous nanorods, nanocubes, and nanooctahedra of ceria prepared by literature procedures were also performed (Figure 2g and Figure S6a-c).[29, 42] First, the surface areas of *PN*-Ceria-160 and *PN*-Ceria-R-160 were 141 m^2/g and 134 m^2/g, increased by 52% and 44% over that of the untreated precursor at 93 m^2/g, respectively. Those values are also significantly larger than those reported for nanoparticles (82.4 m^2/g), non-porous nanorods (107 m^2/g), nanocubes (12.2 m^2/g), or nanooctahedra (8.4 m^2/g) as the surface area is the sum of all available within the porous structures and is not limited to the "exterior" of the non-porous nanorods.

We then analyzed the oxidation states of the Ce ions by X-ray

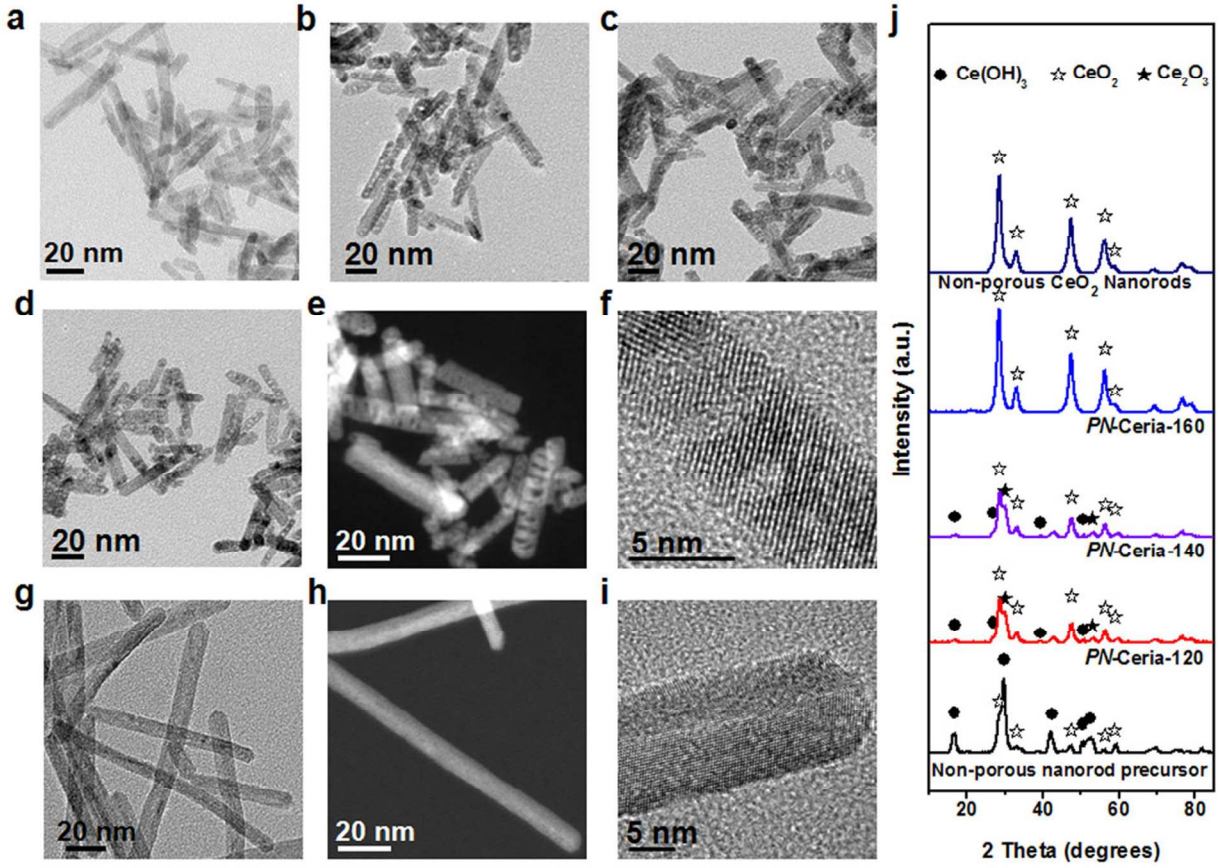

Fig. 2 Structural characterization of porous and non-porous CeO_2 nanorods. a, TEM image of the non-porous nanorod precursor. b, TEM image of *PN*-CeO_2-120. c, TEM image of *PN*-CeO_2-140. d, TEM image of *PN*-CeO_2-160. e, Dark field TEM image of *PN*-CeO_2-160. f, HRTEM image of *PN*-CeO_2-160. g, TEM image of non-porous CeO_2 nanorods. h, Dark field TEM image of non-porous CeO_2 nanorods. i, HRTEM image of non-porous CeO_2 nanorods. j, XRD patterns of ceria-based nanostructures.

photoelectron spectroscopy (XPS) as the fraction of surface-bound vacancies, a parameter key to the catalytic applications of nanoceria-based materials. The eight peaks shown in Figure 3a correspond to four pairs of spin-orbit doublets associated with the 3d electrons of Ce,[43] based on which the fraction of Ce^{3+} in *PN*-Ceria-160 was estimated to be 30.8% (Table 1 and Figure S7); this value is larger than that of *PN*-Ceria-R-160 (21.6%), and is higher than that of non-porous nanorods (14.5%), nanocubes (16.7%), or nanooctahedra (19.0%) of ceria. However, part of borosilicate could be dissolved in such a high concentration of sodium hydroxide.[44] Fortunately, no peak in the range of 96-113 ev was observed where the binding energy peak characteristic of Si would show as in the case of the control sample of a silicon pellet (Figure S8). Thus, the obtained porous nanorods of ceria is free of Si even though the synthesis was carried out in a borosilicate Pyrex tube with the use of high concentration NaOH.

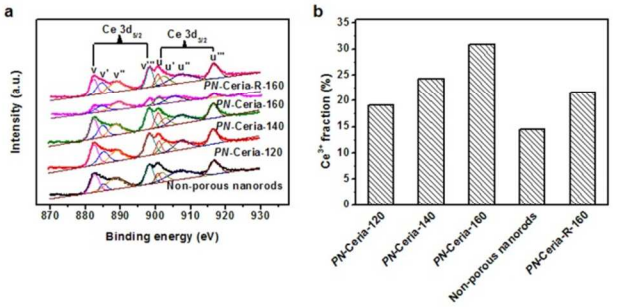

Fig. 3 XPS analysis of CeO_2 nanorods. a, XPS detail spectra of the Ce 3d core level regions for all cerium-based nanorods. b, Surface Ce^{3+} fraction of each CeO_2 nanorods.

The higher density of surface-bound oxygen vacancies in the present porous nanorods is further supported by comparative to Raman spectroscopic studies (Figure S9). The main peak at 459 cm^{-1} corresponds the symmetrical stretching of the cubic fluorite unit, while the peak of interest at 600 cm^{-1} indicates the presence of oxygen vacancies in the nanocrystalline ceria lattice.[45] Consistent with the conclusion by XPS studies, both *PN*-Ceria-160 and *PN*-Ceria-R-160 exhibit a stronger peak at 600 cm^{-1} than their non-porous analogue, suggesting a higher density of oxygen vacancies on the surface of porous CeO_2 nanorods.

The reducibility of porous CeO_2 nanorods was evaluated using the temperature-programmed reduction (TPR) by CO in the temperature range of 50 to 800 °C. The profile of evolved CO_2 against those produced with the use of various forms of previously reported nanoceria are shown in Figure 4a, from which two distinct temperature windows, below and above 370 °C, and corresponding respectively to the reduction of the surface active oxygen species

Table 1. Structural information and catalytic performance of nanocerias for CO oxidation

Sample	Ce^{3+} fraction (%)	BET (m^2/g)[a]	OSC (μmol O_2/g)[b]	T_{50} (°C)[c]	T_{90} (°C)[c]	T_{99} (°C)[c]
PN-Ceria-120	19.1	109	-	-	-	-
PN-Ceria-140	24.3	120	-	-	-	-
PN-Ceria-160	30.8	141	900.2	233	271	286
PN-Ceria-R-160	21.6	137	831.2	233	268	292
Non-porous nanorods	14.5	107	167.9	244	300	>420
Nanocubes	16.7	12.2	84.2	341	400	>420
Nanooctahedra	19.0	8.4	152.7	>420	-	-

[a] BET results were determined by the ASAP 2020, Micromeritics Inc. [b] OSC tests were carried out at 400 °C after 1 h H_2 reduction at 550 °C using the CHEMBET-3000, Quantachrome Inc. [c] The values are derived from the light-off curves for the catalysts.

(e.g. oxygen vacancies, surface lattice oxygen) and the removal of the surface hydroxyl groups and interior lattice oxygen are identified.[23] The CO_2 signals in the lower-temperature region from the CO-TPR of *PN*-Ceria-160 and *PN*-Ceria-R-160 are much more intense than that produced with the use of non-porous nanorods, nanocubes, or nanooctahedra of ceria, clearly indicating the much higher concentration of surface-bound active oxygen in *PN*-Ceria-160 and *PN*-Ceria-R-160.

In addition to high reducibility, the applications of ceria-based materials, in particular toward catalytic conversion of automobile exhaust gas, also depends on their oxygen storage capacity (OSC).[6, 12, 31, 35] Impressively, *PN*-Ceria-160 displayed an OSC of 900.2 μmol O_2/g, which is the largest amongst the values reported for any other nanostructured forms of ceria (Table S1), and is only second to the highest value of 934 μmol O_2/g achieved by a Zr-doped ceria.[33] The measured value of OSC (831.2 μmol O_2/g) for *PN*-Ceria-R-160 is also significantly larger than those for non-porous ceria nanostructures, indicating higher activity of the porous CeO_2 nanorods in the catalytic oxidation of CO.

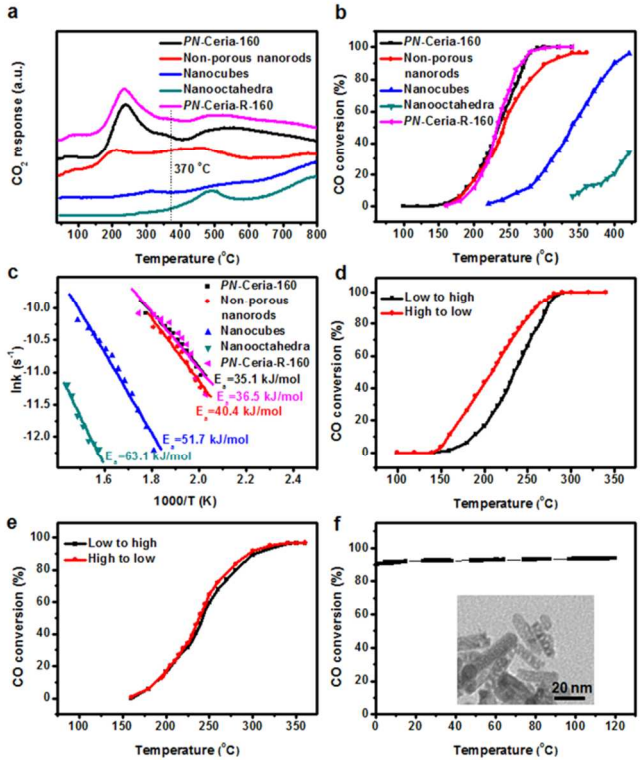

Fig. 4 CO oxidation performance of CeO_2 nanostructures. a, CO_2 evolution profiles during CO-TPR over the catalysts. b, CO oxidation catalyzed by *PN*-CeO_2-160, *PN*-CeO_2-R-160, non-porous CeO_2 nanorods, CeO_2 nanocubes and CeO_2 nanooctahedra. c, The corresponding Arrhenius plot for the five nanoceria catalysts in b. d, Temperature hysteresis of CO conversion on *PN*-CeO_2-160. e, Temperature hysteresis of CO conversion on non-porous CeO_2 nanorods. f, Stability of *PN*-Ceria-160 for CO oxidation at 270 °C. Inset is the TEM image of *PN*-Ceria-160 after 120 hour stream-on-line running.

It is well known that measured OSC in repeated redox cycles can confirm whether the output signals really show catalytic activity or decomposition of nanostructure during heat treatment. Therefore, we obtained OSC data of *PN*-Ceria-160 with the same sample over 6 reduction/oxidation cycles. The reported value of OSC is the average of 6 measurements (903.4, 918.3, 906.6, 893.2, 889.0 and 890.5 μmol O_2/g) (Figure 5a). These results show that this nanoporous structure has a good capacity of storage/release oxygen with excellent recyclability over the redox cycles without apparent degradation. The TEM image (Figure 5b) of the unaltered morphology of *PN*-Ceria-160 illustrates the structural stability of the catalyst.

The catalytic potential of *PN*-Ceria-160 and *PN*-Ceria-R-160 was subsequently assessed. We studied the oxidation of CO (Figure 4b) catalyzed by porous CeO_2 nanorods, with reference to non-porous nanorods, nanocubes, or nanooctahedra under otherwise identical conditions. Commonly accepted for CO oxidation on metal oxides is the two-step Mars-van Krevelen mechanism that entails the adsorption of CO to the surface Ce^{3+} sites, its activation and reaction with lattice oxygen to form the surface COO* intermediates, release of CO_2 accompanied by the generation of oxygen vacancies, and annihilation of the oxygen vacancies by O_2 reactant that is activated on the nanoceria surface.[24, 46] *PN*-Ceria-R-160 exhibited lower

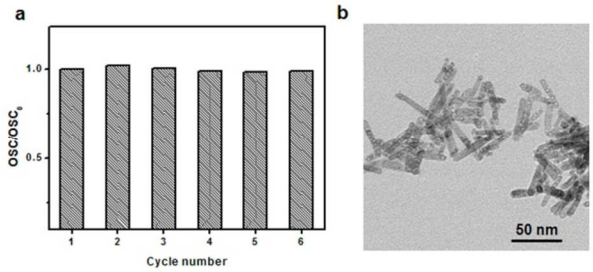

Fig. 5 Oxygen storage/release performance of *PN*-CeO_2-160 in reduction/oxidation cycling test. a, OSC of *PN*-CeO_2-160 in reduction/oxidation cycling test. b, TEM image of *PN*-CeO_2-160 undergo 6 cycle of reduction/oxidation test.

activity for CO oxidation comparable to that of *PN*-Ceria-160, as revealed in their light-off curve (Figure 4b), and both showed much higher activities than the other forms of nanoceria. As presented in Figure 4c, the corresponding Arrhenius plots for the four nanoceria catalysts in Figure 4b revealed that the apparent activation energy of *PN*-Ceria-160 was 35.1 kJ/mol, smaller than the values of 40.4, 51.7 and 63.1 kJ/mol for the non-porous nanorods, nanocubes, and nanooctahedra, respectively. This piece of result suggests that the abundant surface Ce^{3+} and corresponding oxygen vacancies, and the high reducibility of porous nanorods of CeO_2 provide more active sites for CO oxidation than the other forms of nanoceria. This conclusion is also consistent with the lower onset temperature for CO oxidation as well as the lower temperatures of T_{50}, T_{90}, and T_{99} at which 50%, 90%, and 99% of CO were oxidized, respectively (Table 1). For example, with the use of *PN*-Ceria-160, these temperatures are 233, 271, and 286 °C, respectively, each being lower than the corresponding values of 244, 300, and 420 °C when non-porous nanorods were used as catalyst. The enhanced activity of *PN*-Ceria-160 over its non-porous analogues for CO oxidation is thus inferred, reflecting the higher fraction of surface Ce^{3+} and accompanying higher concentration of oxygen vacancies in the present porous nanoceria.

We have also compared the performance of porous nanorods with conventional nanoparticles by calcinating $Ce(NO_3)_3$ under aerobic condition.[7] The particles with a size of 5-10 nm (Figure S6c) possess a surface area of 82.4 m^2/g, a value slightly smaller than the value found for non-porous nanorods of ceria (107 m^2/g), but significantly smaller than the present porous nanorods of ceria at 137 and 141 m^2/g. In addition, T_{50}, T_{90}, and T_{99} of nanoparticles are 274, 315, and 340 °C, respectively (Figure S10a), comparable to the corresponding values with the use of non-porous CeO_2 nanorods (244, 300, and 420 °C), but much inferior to the performance of the present porous nanorods of ceria (233, 271, and 286 °C). These results confirm the enhanced performance of our porous nanorods of ceria.

After light-off measurement from low to high temperature, the catalytic activity of *PN*-Ceria-160 and non-porous CeO_2 nanorods was also evaluated by a subsequent cooling process. As anticipated, there exists a hysteresis between these two measurements (Figure 4d-e), which is similar to those observed in metal/metal oxide catalysts for CO oxidation.[47, 48] Such a hysteresis is rationalized in terms of the "overheating of active sites of the catalysts when decreasing temperature of reactor chamber".[48] The width of the hysteresis directly reflects the activity of the catalysts, with a larger width being associated with a more active catalyst. The width of the temperature hysteresis for 50% of CO conversion is 25 °C and 4 °C for *PN*-Ceria-160 and nonporous CeO_2 nanorods, respectively, clearly suggesting the higher activity of *PN*-Ceria-160 catalyst for CO oxidation.

PN-Ceria-160 exhibits excellent catalytic stability for CO oxidation. We tested the CO-to-CO_2 conversion at 90% level (T_{90} = 270 °C) up to 120 hours, from which the stability of the catalyst is firmly established as the percentage of conversion remained almost constant over this time period. Quite impressively, no significant deterioration of the catalyst was observed even when the reaction is extended beyond the 120-hour period (inset, Figure 4f), providing further evidence of the stability of this porous nanoceria catalyst. Physically, the porous structure and rod-like morphology survived through the harsh conditions such as an ultra-high pressure of 15 MPa for the making of 60-100 mesh catalyst particles by mechanical extrusion, long-term high temperature catalysis at 270 °C over 120 h, and subsequent strong sonication for preparing the TEM sample.

Conclusions

In summary, by adopting a two-step hydrothermal synthesis, porous nanorods - a novel form of nanostructured ceria – have been obtained. As compared with the previously reported preparation of non-porous nanoceria, we found that the relatively low reaction pressure is critical for the formation of a $Ce(OH)_3$ doped CeO_2 precursor. A subsequent step of dehydration and oxidation of the decomposition products led to the production of porous nanorods of ceria that are characterized with significantly increased surface area and structural defects when compared with three other forms of nanoceria (non-porous nanorods, nanocubes, and nanooctahedra). The porosity and surface area of the porous nanorods of CeO_2 show a strong correlation to the weight percentage of $Ce(OH)_3$ in the precursor nanorods, which is determined by pressure in the first step hydrothermal. A much higher fraction of Ce^{3+} was determined that corresponds to a higher number of oxygen vacancies that are responsible for the catalytic activity. Comparative studies of ceria-catalyzed oxidation of CO using various ceria-catalysts clearly demonstrated the much enhanced catalytic power of the high-surface area porous nanorods. The results presented in this work collectively points to the strong correlation between the high surface area, large number of structural defects, and high faction of Ce^{3+} in ceria-based materials and their catalytic performance. With the ease of preparation, practical and useful applications of such porous nanoceria as improved supports, promoters, and active components in various catalyzed oxidation reactions may be envisioned, and so are their ultimate industrial applications.

Acknowledgements

We acknowledge the financial support from a NSFC Grant 21201138. This work was also partially funded from the Ministry of Science and Technology of China through a 973-program under Grant 2012CB619401 and the Fundamental Research Funds for the Central Universities. Technical supports for TEM experiments from TEM Laboratory of Frontier Institute of Science and Technology and from State Key Laboratory for Manufacturing Systems Engineering, Xi'an Jiaotong University, are also acknowledged.

Notes and references

[a] *Center for Applied Chemical Research, Frontier Institute of Science and Technology, Xi'an Jiaotong University, Xi'an, China, 710049. E-mail: yongquan@mail.xjtu.edu.cn*
[b] *Institute of Chemistry for New Energy Materials, Department of Chemistry, Xi'an Jiaotong University, Xi'an, China 710049.*
[c] Department of Chemistry and Biochemistry, University of Arizona, Tucson, Arizona 85721
†Electronic Supplementary Information (ESI) available: [XRD patterns, XPS spectra, more TEM images, and other data.]. See DOI: 10.1039/b000000x/

1. C. Sun, H. Li and L. Chen, *Energy Environ. Sci.*, 2012, **5**, 8475-8505.
2. L. Vivier and D. Duprez, *ChemSusChem*, 2010, **3**, 654-678.
3. M. Mogensen, N. M. Sammes and G. A. Tompsett, *Solid State Ionics*, 2000, **129**, 63-94.
4. H. Wei and E. Wang, *Chem. Soc. Rev.*, 2013, **42**, 6060-6093.
5. Q. Yuan, H.-H. Duan, L.-L. Li, L.-D. Sun, Y.-W. Zhang and C.-H. Yan, *J. Colloid Interface Sci.*, 2009, **335**, 151-167.
6. J. Kašpar, P. Fornasiero and M. Graziani, *Catal. Today*, 1999, **50**, 285-298.
7. M. Cargnello, V. V. T. Doan-Nguyen, T. R. Gordon, R. E. Diaz, E. A. Stach, R. J. Gorte, P. Fornasiero and C. B. Murray, *Science*, 2013, **341**, 771-773.
8. A. Primo, T. Marino, A. Corma, R. Molinari and H. García, *J. Am. Chem. Soc.*, 2011, **133**, 6930-6933.
9. C. Wen, Y. Zhu, Y. Ye, S. Zhang, F. Cheng, Y. Liu, P. Wang and F. (F.) Tao, *ACS Nano*, 2012, **6**, 9305-9303.
10. W. Xu, Z. Liu, A. C. Johnston-Peck, S. D. Senanayake, G. Zhou, D. Stacchiola, E. A. Stach and J. A. Rodriguez, *ACS Catal.*, 2013, **3**, 975-984.
11. Q. Fu, H. Saltsburg and M. Flytzani-Stephanopoulos, *Science*, 2003, **301**, 935-938.
12. G. Li, Q. Wang, B. Zhao, M. Shen and R. Zhou, *J. Hazard. Mater.*, 2011, **186**, 911-920.
13. J. A. Farmer and C. T. Campbell, *Science*, 2010, **329**, 933-936.
14. Q. Yuan, H.-H. Duan, L.-L. Li, Z.-X. Li, W.-T. Duan, L.-S. Zhang, W.-G. Song and C.-H. Yan, *Adv. Mater.*,2010, **22**, 1475-1478.
15. K. An, S. Alayoglu, N. Musselwhite, S. Plamthottam, G. Melaet, A. E. Lindeman and G. A. Somorjai, *J. Am. Chem. Soc.*, 2013, **135**, 16689-16696.
16. N. J. Lawrence, J. R. Brewer, L. Wang, T.-S. Wu, J. Wells-Kingsbury, M. M. Ihrig, G. Wang, Y.-L. Soo, W.-N. Mei and C. L. Cheung, *Nano Lett.*, 2011, **11**, 2666-2671.
17. N. Ta, J. (J.) Liu, S. Chenna, P. A. Crozier, Y. Li, A. Chen and W. Shen, *J. Am. Chem. Soc.*, 2012, **134**, 20585-20588.
18. F. Esch, S. Fabris, L. Zhou, T. Montini, C. Africh, P. Fornasiero, G. Comelli and R. Rosei, *Science*, 2005, **309**, 752-755.
19. F. C.; Calaza, Y. Xu, D. R. Mullins and S. H. Overbury, *J. Am. Chem. Soc.*, 2012, **134**, 18034-18045.
20. C. T. Campbell and C. H. F. Peden, *Science*, 2005, **309**, 713-714.
21. X. Liu, K. Zhou, L. Wang, B. Wang and Y. Li, *J. Am. Chem. Soc.*, 2009, **131**, 3140-3141.
22. T. Taniguchi, K. Katsumata, S. Omata, K. Okada and N. Matsushita, *Cryst. Growth Des.*, 2011, **11**, 3754-3760.
23. Z. Wu, M. Li and S. H. Overbury, *J. Catal.*, 2012, **285**, 61-73.
24. H. Y. Kim, H. M. Lee and G. Henkelman, *J. Am. Chem. Soc.*, 2012, **134**, 1560-1570.
25. Y. Sun, Q. Liu, S. Gao, H. Cheng, F. Lei, Z. Sun, Y. Jiang, H. Su, S. Wei and Y. Xie, *Nat. Commun.*, 2013, DOI: 10.1038/ncomms3899.
26. W.Q. Han, L. Wu and Y. Zhu, *J. Am. Chem. Soc.*, 2005, **127**, 12814-12815.
27. N. Acerbi, S. C. Edman Tsang, G. Jones, S. Golunski and P. Collier, *Angew. Chem. Int. Ed.*, 2013, **52**, 1-6.
28. E. Mamontov, T. Egami, R. Brezny, M. Koranne and S. Tyagi, *J. Phys. Chem. B*, 2000, **104**, 11110-11116.
29. H.-X. Mai, L.-D. Sun, Y.-W. Zhang, R. Si, W. Feng, H.-P. Zhang, H.-C. Liu and C.-H. Yan, *J. Phys. Chem. B*, 2005, **109**, 24380-24385.
30. J. Ke, J.-W. Xiao, W. Zhu, H. Liu, R. Si, Y.-W. Zhang and C.-H. Yan, *J. Am. Chem. Soc.*, 2013, **135**, 15191-15200.
31. G. Li, Q. Wang, B. Zhao and R. Zhou, *Appl. Catal. B*, 2011, **105**, 151-162.
32. W. Cai, F. Wang, C. Daniel, A. C. van Veen, Y. Schuurman, C. Descorme, H. Provendier, W. Shen and C. Mirodatos, *J. Catal.*, 2012, **286**, 137-152.
33. S. Letichevsky, C. A. Tellez, R. R. de Avillez, M. I. P. da Silva, M. A. Fraga and L. G. Appel, *Appl. Catal. B*, 2005, **58**, 203-210.
34. J. Zhang, H. Kumagai, K. Yamamura, S. Ohara, S. Takami, A. Morikawa, H. Shinjoh, K. Kaneko, T. Adschiri and A. Suda, *Nano Lett.*, 2011, **11**, 361-364.
35. K. Yamazaki, N. Takahashi, H. Shinjoh and M. Sugiura, *Appl. Catal. B*, 2004, **53**, 1-12.
36. C. Sun, H. Li, H. Zhang, Z. Wang and L. Chen, *Nanotechnology*, 2005, **16**, 1454-1463.
37. F. Zhang, S.-W. Chan, J. E. Spanier, E. Apak, Q. Jin, R. D. Robinson and I. P. Herman, *Appl. Phys. Lett.*, 2002, **80**, 127-129.
38. D. Wang, Y. Kang, V. Doan-Nguyen, J. Chen, R. Küngas, N. L. Wieder, K. Bakhmutsky, R. J. Gorte and C. B. Murray, *Angew. Chem. Int. Ed.*, 2011, **50**, 4378-4381.
39. A. Gayen, K. R. Priolkar, P. R. Sarode, V. Jayaram, M. S. Hegde, G. N. Subbanna and S. Emura, *Chem. Mater.*, 2004, **16**, 2317-2328.
40. Q. Wang, G. Li, B. Zhao, M. Shen and R. Zhou, *Appl. Catal. B*, 2010, **101**, 150-159.
41. B. Coasne, A. Grosman, C. Ortega, and M. Simon, *Phys. Rev. Lett.,* 2002, **88**, 256102.
42. L. Feng, D. T. Hoang, C.-K. Tsung, W. Huang, S. H.-Y. Lo, J. B. Wood, H. Wang, J. Tang and P. Yang, *Nano Res.*, 2011, **4**, 61-71.
43. M. A. Henderson, C. L. Perkins, M. H. Engelhard, S. Thevuthasan and C. H. F. Peden, *Surf. Sci.*, 2003, **526**, 1-18.
44. R. D. Smith and P. E. Corbin, *J. Am. Ceram. Soc.*, 2006, **32**, 195-198.
45. Y. Lee, G. He, A. J. Akey, R. Si, M. Flytzani-Stephanopoulos and I. P. Herman, *J. Am. Chem. Soc.*, 2011, **133**, 12952-12955.
46. G. G. Jernigan and G. A. Somorjai, *J. Catal.*, 1994, **147**, 567-577.
47. L. D. Rogatis, M. Cargnello, V. Gombac, B. Lorenzut, T. Montini and P. Fornasiero, *ChemSusChem*, 2010, **3**, 24-42.
48. A. N. Subbotin, B. S. Gudkov, Z. L. Dykh and V. L. Yakerson, *React. Kinet. Catal. Lett.*, 1999, **66**, 97-104.

Low Pressure Induced Porous Nanorods of Ceria with High Reducibility and Large Oxygen Storage Capacity: Synthesis and Catalytic Applications

Jing Li,[a] Zhiyun Zhang,[a] Zhimin Tian,[a] Xuemei Zhou,[a] Zhiping Zheng,[a, b, c] Yuanyuan Ma,[a, b] Yongquan Qu*[a, b]

[a] *Center for Applied Chemical Research, Frontier Institute of Science and Technology, Xi'an Jiaotong University, Xi'an, 710049, China*

[b] *Institute of Chemistry for New Energy Materials, Department of Chemistry, Xi'an Jiaotong University, Xi'an, China 740049.*

[c] *Department of Chemistry and Biochemistry, University of Arizona, Tucson, Arizona 85721*

E-mail: yongquan@mail.xjtu.edu.cn

A new form of nanoceria, porous nanorods of ceria (*PN*-CeO_2), was prepared by a two-step hydrothermal synthesis. The *PN*-CeO_2 has been found to display enhanced reducibility and capacity for oxygen storage (900.2 μmol O_2/g) as a result of their significantly increased surface area and defects over other forms of nanoceria, including nanoparticles, non-porous nanorods, nanocubes, and nanooctahedra. The high catalytic activity of *PN*-CeO_2 for CO oxidation indicates their potentials as the catalysts or supports or promoters for advanced oxidative processes for waste treatment and environmental remediation.